

Quantum-critical spin dynamics in quasi-one-dimensional antiferromagnets

S. Mukhopadhyay,¹ M. Klanjšek,^{1,2,3,*} M. S. Grbić,^{1,4} R. Blinder,¹ H. Mayaffre,¹ C. Berthier,¹
M. Horvatić,^{1,†} M. A. Continentino,⁵ A. Paduan-Filho,⁶ B. Chiari,⁷ and O. Piovesana⁷

¹*Laboratoire National des Champs Magnétiques Intenses, LNCMI - CNRS (UPR3228),
UJF, UPS and INSA, BP 166, 38042 Grenoble Cedex 9, France*

²*Jožef Stefan Institute, Jamova 39, 1000 Ljubljana, Slovenia*

³*EN-FIST Centre of Excellence, Dunajska 156, 1000 Ljubljana, Slovenia*

⁴*Department of Physics, Faculty of Science, University of Zagreb, PP 331, HR-10002 Zagreb, Croatia*

⁵*Centro Brasileiro de Pesquisas Físicas, 22290-180 Rio de Janeiro, Brazil*

⁶*Universidade de São Paulo, 05315-970 São Paulo, Brazil*

⁷*Dipartimento di Chimica, Università di Perugia, I-06100, Perugia, Italy*

(Dated: August 31, 2012)

By means of nuclear spin-lattice relaxation rate T_1^{-1} , we follow the spin dynamics as a function of the applied magnetic field in two gapped one-dimensional quantum antiferromagnets: the anisotropic spin-chain system $\text{NiCl}_2\text{-4SC(NH}_2)_2$ and the spin-ladder system $(\text{C}_5\text{H}_{12}\text{N})_2\text{CuBr}_4$. In both systems, spin excitations are confirmed to evolve from magnons in the gapped state to spinons in the gapless Tomonaga-Luttinger-liquid state. In between, T_1^{-1} exhibits a pronounced, continuous variation, which is shown to scale in accordance with quantum criticality. We extract the critical exponent for T_1^{-1} , compare it to the theory, and show that this behavior is identical in both studied systems, thus demonstrating the universality of quantum critical behavior.

PACS numbers: 75.10.Pq, 64.60.F-, 75.40.Gb, 76.60.-k

Quantum phase transitions are currently in the focus of condensed-matter physics [1–4]. In contrast to classical phase transitions, driven by thermal fluctuations, quantum phase transitions are driven by quantum fluctuations that can be tuned by non-thermal control parameters, like the magnetic field, pressure or chemical composition. The influence of a quantum critical point (QCP), where the continuous quantum phase transition occurs at zero temperature, extends to a broad V-shaped region of quantum criticality at non-zero temperatures (like in Fig. 1). A complex physics in this region is universal, i.e., insensitive to the microscopic properties of the system, and scale invariant, with temperature setting the only energy scale. Quantum phase transitions have been experimentally studied in heavy-fermion metals [4, 5], magnetic insulators [6–9] and cold atoms [10, 11]. Magnetic insulators exhibit relatively simple and well-defined Hamiltonians and allow for powerful local probes accessing spin statics and dynamics, like neutron scattering [7–9] and nuclear magnetic resonance (NMR) [12]. Nevertheless, a clear experimental demonstration of the quantum critical behavior in magnetic insulators is still missing.

Particularly convenient are systems of weakly coupled one-dimensional (1D) gapped antiferromagnets [13], like spin chains or ladders, for two reasons. First, the applied magnetic field B simply controls the gap between the ground state and the lowest spin excitations, i.e., magnons. If Δ is the zero-field gap, this gap closes at the critical field $B_{c1} = \Delta/(g\mu_B)$, which defines the QCP (μ_B is Bohr magneton). Beyond this QCP, magnons fractionalize into pairs of spinons [8], characteristic of the gapless, Tomonaga-Luttinger-liquid (TLL) ground state [12, 14]. Second, weakly coupled spin chains or

ladders feature well separated temperature scales relevant for the physics in 3D and 1D. These are characterized respectively by the corresponding weak, 3D exchange couplings J_{3D} and the dominant, 1D exchange coupling J (Fig. 1). In particular, in the temperature range $k_B T < J_{3D}$ (k_B is Boltzmann constant), 3D couplings lead to the 3D ordered state in the TLL region [12]. In the range $J_{3D} < k_B T < J$, the physics gradually becomes 1D, while above J the 1D identity of the system is lost. As sketched in Fig. 1, crossover temperatures to both the gapped and TLL regions depend linearly on $B - B_{c1}$ around the QCP [15]. They outline a char-

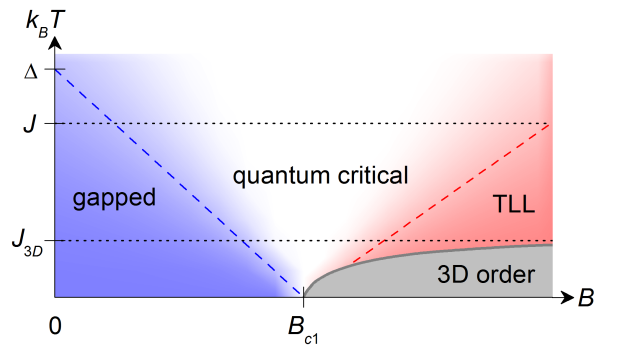


FIG. 1: (color online) Characteristic field-temperature phase diagram of weakly coupled, gapped antiferromagnetic chains or ladders around the critical field B_{c1} that closes the gap. The slopes $-g\mu_B$ and $0.76g\mu_B$ [15] of the temperature crossovers to the gapped and TLL regions, respectively, are indicated by dashed lines. Dotted lines indicate characteristic temperature scales set by the dominant, 1D coupling J and weak, 3D couplings J_{3D} .

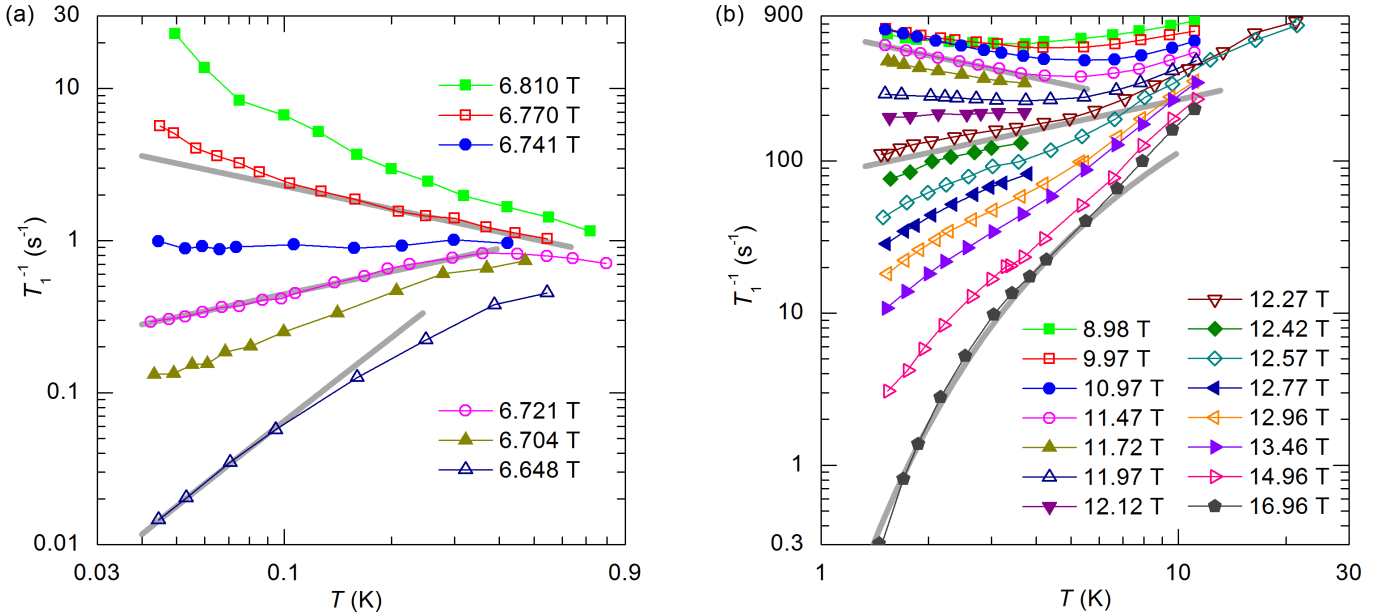


FIG. 2: (color online) T_1^{-1} as a function of temperature T for several magnetic field values around the QCP. (a) In BPCB, ^{14}N T_1^{-1} data are taken around $B_{c1} = 6.723$ T on $\text{N}(1)_{\text{II}}$ NMR lines as defined in Ref. [12]. The value of B_{c1} is determined from the low-temperature magnetization as measured by ^{14}N NMR hyperfine shift. (A more precise determination provides a slightly higher value than reported in Ref. [12].) (b) In DTN, proton T_1^{-1} data are taken around $B_{c2} = 12.325$ T on the highest-frequency NMR line. Magnetic field is aligned with the c axis to within 1° . The value of B_{c2} is determined from the low-temperature boundary $T_c(B)$ of the 3D ordered state as measured by proton NMR [24]. Thick gray lines in (a) and (b) are $T_1^{-1}(T)$ predictions for the TLL behavior close to the critical field ($T_1^{-1} \propto T^{-1/2}$), for the tentative quantum critical behavior exactly at the critical field ($T_1^{-1} \propto T^{1/2}$), and for the gapped behavior, from top to bottom, respectively.

acteristic V-shaped quantum critical region in the field-temperature phase diagram [16]. Spin dynamics in this region has not been systematically explored yet.

We explore the quantum-critical spin dynamics in two particularly clean and convenient model systems: $\text{NiCl}_2\text{-4SC}(\text{NH}_2)_2$ (DTN) containing chains of $S = 1$ spins subject to a single-ion anisotropy [17–19], and $(\text{C}_5\text{H}_{12}\text{N})_2\text{CuBr}_4$ (BPCB) containing spin-1/2 ladders [8, 12, 16, 20, 21]. Both compounds feature experimentally accessible critical fields, while the crystal symmetry assures the absence of the antisymmetric Dzyaloshinskii-Moriya interaction that could perturb the closing of the gap at the QCP. In the strong-coupling approximation [12], where only the two spin states that close the gap are kept (among four rung states for the ladder and three spin states for the chain), both systems are described by the same effective spin-1/2 XXZ chain model with the coupling anisotropy $J_Z/J_{X,Y} = 0.5$. Accordingly, they exhibit a similar phase diagram, which contains also the second QCP at the critical field B_{c2} that separates the gapless state from a gapped, fully polarized state [8, 12, 16, 18–21]. While the 1D couplings are comparable in both compounds, their 3D couplings differ by an order of magnitude (Table I). A comparison of the quantum critical behavior in both compounds thus offers a severe test of universality. Indeed, our results allow us to demonstrate (i) the universality and (ii) scale in-

variance of the quantum-critical spin dynamics, and (iii) extract the critical exponent for T_1^{-1} , which is compared to the existing theoretical predictions [22].

Nuclear spin-lattice relaxation rate T_1^{-1} measurements allow us to monitor the spin dynamics around the QCP in both compounds to high precision and in great detail. Namely, T_1^{-1} can cover many orders of magnitude keeping the same precision, while the magnetic field B as a tuning parameter can be easily controlled. T_1^{-1} provides a direct access to the low-energy spin excitations, as it probes nearly zero-energy limit of the local (i.e., momentum integrated) spin-spin correlation function [23]. Fig. 2 shows $T_1^{-1}(T)$ datasets for various magnetic field

	J_0	J	J/J_0	J_{3D}	T_{3D}^{max}
BPCB	12.9	3.6	0.28	0.08	0.11
DTN	8.9	4.4	0.49	0.72	1.2

TABLE I: The exchange couplings in the effective spin-1/2 XXZ chain model for BPCB (DTN): on-site coupling J_0 is the rung coupling J_\perp (single-ion anisotropy D), 1D coupling J is the leg coupling J_\parallel (intrachain coupling $2J_c$), 3D coupling J_{3D} is the interladder coupling zJ' with $z = 4$ (interchain coupling $zJ_{a,b}$ with $z = 4$), and the highest transition temperature T_{3D}^{max} to the 3D ordered state, all in kelvin units [12, 19].

values around the QCP. In BPCB, the datasets taken around B_{c1} exhibit a power-law behavior, $T_1^{-1} \propto T^\alpha$ (i.e., they are linear in a log-log scale), over nearly a decade [Fig. 2(a)]. The exponent α varies rapidly across the critical field, resulting in a fan-like pattern of the data. At low temperature, the power-law (i.e., linear) behavior is modified at the lowest field value by the gap opening, which reduces T_1^{-1} , and at the two highest field values by the 3D critical fluctuations, which enhance T_1^{-1} close to the boundary $T_c(B)$ of the 3D ordered state [12]. At high temperature, the deviation from the power-law behavior starts above 0.3 K, where all the datasets assume a decreasing trend. After passing a broad minimum starting at 4 K, which is comparable to J in BPCB (Table I), the relaxation starts to increase towards the high-temperature paramagnetic limit (not shown). Because of the low B_{c1} value in DTN, the $T_1^{-1}(T)$ data are instead taken around B_{c2} , and they exhibit essentially the same power-law fan-like pattern as in BPCB [Fig. 2(b)], although limited to a narrower temperature range below 4 K. Above this temperature, which is comparable to J in DTN (Table I), the relaxation directly starts to increase to the high-temperature paramagnetic regime. The low-temperature behavior again reflects entering into the gapped, this time fully polarized region at the high field values, while the divergence of relaxation at the low field values, close to $T_c(B)$, is not visible, as the lowest covered temperature of 1.5 K is not close enough to the 3D ordered state [$T_c(10\text{ T}) = 0.9\text{ K}$].

The limits of this fan-like pattern in Figs. 2(a) and (b) are easily understood and reflect the nature of the low-energy spin excitations on each side of the QCP. Namely, in the gapless, TLL region, the two-spinon continuum in a dynamic correlation function leads to the power-law behavior $T_1^{-1} \propto T^{1/(2K)-1}$, where K is the TLL exponent [12, 25]. Approaching the QCP from the TLL side, K gradually increases to 1, meaning that $\alpha = 1/(2K) - 1$ decreases to $-1/2$, which is the lowest expected value of α . As indicated by upper gray lines in Figs. 2(a) and (b), this lowest α value is indeed observed just above B_{c1} in BPCB, for $k_B T > J_{3D}$, and just below B_{c2} in DTN. In the gapped region, magnon excitations over the gap result in an activated behavior $T_1^{-1} \propto T^{\alpha_0} \exp[\pm g\mu_B(B - B_{c1,2})/(k_B T)]$, where $g = 2.176$ for BPCB [12] and 2.26 for DTN [19], the + sign refers to B_{c1} and - to B_{c2} . The exponent α_0 depends on the effective dimension of the magnon dispersion relation as selected by thermal fluctuations $k_B T$. On raising temperature, α_0 gradually decreases from 2 for $k_B T < J_{3D}$ (3D case) towards 0 for $J_{3D} \ll k_B T < J$ (1D case). The $T_1^{-1}(T)$ datasets deepest in the gapped region indeed exhibit this type of low-temperature behavior, with $\alpha_0 = 1.8$ for BPCB (calculated at 0.05 K) and 0.83 for DTN (calculated at 2 K), as shown by lower gray lines in Figs. 2(a) and (b). In between the gapped and TLL regions neither description applies, implying that in the

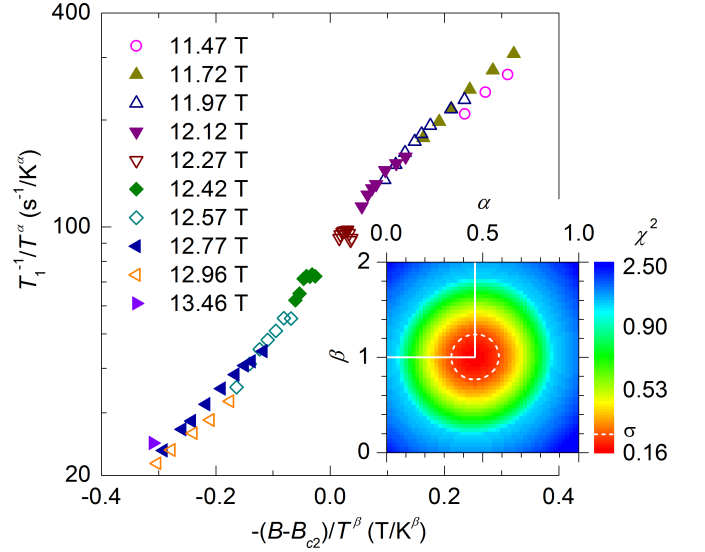


FIG. 3: (color online) Demonstration of the scale invariance in the quantum critical region of DTN. The best collapse of different $T_1^{-1}(T)$ datasets [displayed in Fig. 2(b)] on the same curve in scaling variables $-(B - B_{c2})/T^\beta$ and T_1^{-1}/T^α is obtained for the critical exponents $\alpha = 0.46 \pm 0.12$ and $\beta = 1.00 \pm 0.24$, with mean values used in the plot. Inset shows the color plot of $\chi^2(\alpha, \beta)$ measuring the goodness of this collapse. Obtained mean values are indicated by solid white lines, their uncertainties are given by a standard deviation σ (dashed white contour line).

white region of Fig. 1 spin excitations are neither spinons nor magnons. Interestingly, these excitations lead approximately to $T_1^{-1} \propto T^{1/2}$ exactly at the critical field in both compounds, as indicated by middle gray lines in Figs. 2(a) and (b).

To show that spin excitations in the white region of Fig. 1 are characteristic of quantum criticality, we establish a scaling relation for the T_1^{-1} data in this region. Assuming that T_1^{-1} and the parameter controlling the proximity to a QCP, $\pm(B - B_{c1,2})$, scale as powers α and β of temperature, the scaling relation reads

$$\frac{T_1^{-1}}{T^\alpha} = F \left[\frac{\pm(B - B_{c1,2})}{T^\beta} \right], \quad (1)$$

where F is the scaling function. To check Eq. (1), we first focus on DTN. We crop the ranges of the $T_1^{-1}(T)$ datasets by the constraints $g\mu_B|B - B_{c2}| < 0.5 k_B T$ and $T < 4\text{ K}$ to confine them well to the quantum critical region where the power-law behavior is observed. Then we look for the values of the exponents α and β leading to the best collapse of the cropped datasets on the same curve in scaling variables $-(B - B_{c2})/T^\beta$ and T_1^{-1}/T^α . For a given pair of α and β values, we fit the dataset containing *all* the cropped and scaled datasets by the appropriate analytical function, a third-order polynomial in our case, and use the χ^2 of this fit as a measure of the collapse. As shown in Fig. 3 inset, the minimization of χ^2 as a function of both

exponents leads to $\alpha = 0.46 \pm 0.12$ and $\beta = 1.00 \pm 0.24$. A corresponding excellent collapse of all the datasets on the same curve, shown in Fig. 3, provides a nice demonstration of scale invariance. The energy scale is set only by temperature, and the obtained *linear* scaling of the control parameter $-(B - B_{c2})$ with temperature (i.e., $\beta = 1$) is a clear sign of quantum criticality [1–3]. The same analysis for BPCB, with $T_1^{-1}(T)$ datasets confined to the range between 0.1 K ($\sim J_{3D}/k_B$) and 0.3 K, gives similar values $\alpha = 0.48 \pm 0.06$ and $\beta = 1.04 \pm 0.08$. In both cases, Eq. (1) gives $T_1^{-1} \propto T^\alpha$ with the critical exponent $\alpha \approx 1/2$ *exactly* at the critical field. This result differs from the existing theoretical predictions for the 3D quantum criticality, $\alpha = 3/4$, and for the 1D quantum criticality, $\alpha = -1/2$, both given in Ref. [22]. In the white region in Fig. 1, the first case applies to the range $k_B T < J_{3D}$. This region separates the gapped state from the 3D ordered state, which can be understood as a Bose-Einstein condensate (BEC) of magnons [25–27]. The second case applies to the range $J_{3D} \ll k_B T < J$, where the effect of J_{3D} is negligible. However, our result applies to the middle of the range $J_{3D} < k_B T < J$, which has not been theoretically described yet.

Finally, we show that the similarity of the T_1^{-1} fan-like patterns in both compounds is not only qualitative but also quantitative. For this purpose, from the data displayed in Fig. 2 we extract the *field* variations of T_1^{-1} and of the (effective) power-law exponent $\alpha = \partial \ln(T_1^{-1}) / \partial \ln(T)$ at a given temperature. Having established $\pm(B - B_{c1,2})/T$ as the proper scaling variable in the quantum critical region, we plot in Fig. 4 T_1^{-1} and α in DTN as a function of this variable at $T_{\text{DTN}} = 2$ K. Strong variations of both observables are localized in a narrow range around the QCP, where T_1^{-1} increases by a factor of 10 and α changes from 1.5 to -0.5 from the gapped to the TLL region. Outside the quantum critical region, the observed α versus $\pm(B - B_{c1,2})/T$ variation is nicely reproduced [see Fig. 4(b)] on the basis of T_1^{-1} expressions given above: with $\alpha = \pm g\mu_B(B - B_{c1,2})/(k_B T) + \alpha_0$ on the gapped side, where $\alpha_0 = 0.83$ (calculated at T_{DTN}), and with $\alpha = 1/(2K) - 1$ on the TLL side, where we use $K(B)$ in the strong-coupling approximation [12]. In the quantum critical region, where neither description applies, we look for the temperature T_{BPCB} to achieve the best overlap of the T_1^{-1} and α datasets for BPCB with those for DTN. As shown in Fig. 4(b) inset, the obtained $T_{\text{BPCB}} = 0.18$ K leads to $T_{\text{DTN}}/T_{\text{BPCB}} = 11$. We get the same ratio for any chosen T_{DTN} in the covered temperature range. An excellent overlap of the BPCB datasets with those for DTN, despite different exchange couplings defining their Hamiltonians (Table I), provides a clear demonstration of universality. Spin dynamics in the quantum critical region can be understood in terms of strongly interacting magnons [22]. The characteristic temperature for the magnon-magnon interaction is given by the highest transition temperature T_{3D}^{max} to the 3D

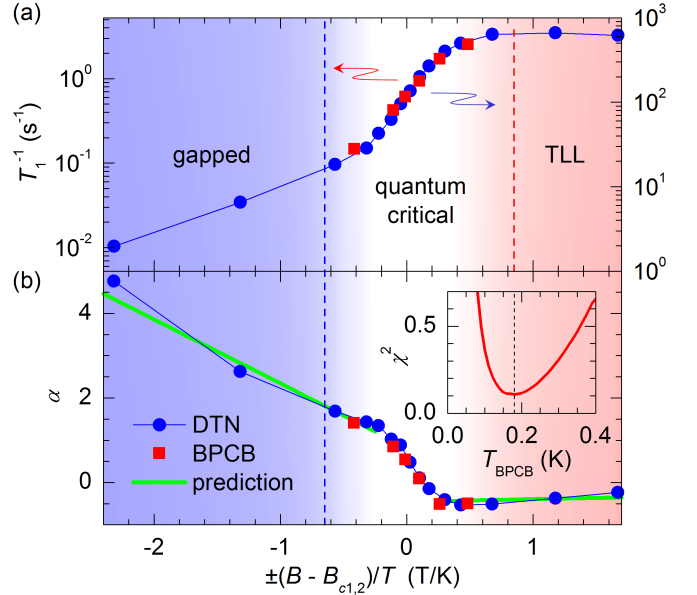


FIG. 4: (color online) Demonstration of the universality of quantum-critical behavior. (a) T_1^{-1} versus $\pm(B - B_{c1,2})/T$ datasets for BPCB at 0.18 K and DTN at 2 K [determined from the data in Figs. 2(a) and (b)] overlap perfectly in the quantum critical region. (b) Corresponding overlap of the α datasets, where the power-law exponents α are evaluated as the slopes of tangents to the $T_1^{-1}(T)$ datasets in a log-log scale. Inset shows the $\chi^2(T_{\text{BPCB}})$ plot measuring the goodness of this overlap at a fixed $T_{\text{DTN}} = 2$ K, defining the optimal $T_{\text{BPCB}} = 0.18$ K (indicated by the dashed line). Dashed lines in (a) and (b) indicate the crossover temperatures to the gapped (blue) and TLL (red) regions, as in Fig. 1, and the green lines in (b) are α versus $\pm(B - B_{c1,2})/T$ predictions in these two regions. Different T_1^{-1} scales in (a) are due to different gyromagnetic ratios and different NMR hyperfine couplings for ^{14}N and protons.

ordered (i.e., BEC) state (see Fig. 1 and Table I). The fact that $T_{3D, \text{DTN}}^{\text{max}}/T_{3D, \text{BPCB}}^{\text{max}} = 11$ precisely corresponds to the obtained $T_{\text{DTN}}/T_{\text{BPCB}}$ indicates that the universality is defined by an interaction-dependent scale factor [13, 28]. In the end, we note that a dataset like those plotted in Fig. 4(a) was obtained for the spin-chain compound CuPzN in Ref. [29], but was interpreted within the TLL framework, which does not apply to the quantum critical region.

In summary, we showed that the quantum-critical spin dynamics in gapped quasi-1D antiferromagnets cannot be understood in terms of spinons or magnons, but rather in terms of more complicated spin excitations. Their behavior was experimentally demonstrated to be scale invariant and universal, where the scale factor is defined by the magnon-magnon interaction. We extracted the critical exponent for T_1^{-1} in the region which is not covered by any theory. For the well developed 3D region at lower temperatures ($k_B T \ll J_{3D}$) and for the 1D region at higher temperatures ($J_{3D} \ll k_B T < J$) theoretical

descriptions exist [13, 22]. As T_1^{-1} can be expressed in terms of the dynamical susceptibility [23], the extension of our experimental study to these regions should allow to extract the universal critical exponents for susceptibility and correlation length in 1D and 3D, and compare them to existing theories.

We acknowledge fruitful discussions with T. Giamarchi. Part of this work has been supported by the French ANR project NEMSICOM, by EuroMagNET network under the EU contract No. 228043, by the ARRS project No. J1-2118, and by the EU FP7 project SOLen-eMaR N 229390.

* Electronic address: martin.klanjsek@ijs.si

† Electronic address: mladen.horvatic@lncmi.cnrs.fr

- [1] S. Sachdev, *Quantum Phase Transitions* (Cambridge University Press, 1999).
- [2] P. Coleman and A. J. Schofield, *Nature* **433**, 226 (2005).
- [3] S. Sachdev and B. Keimer, *Phys. Today* **64**, 29 (2011).
- [4] Q. Si and F. Steglich, *Science* **329**, 1161 (2010).
- [5] A. Schröder *et al.*, *Nature* **407**, 351 (2000).
- [6] S. E. Sebastian *et al.*, *Nature* **441**, 617 (2006).
- [7] Ch. Rüegg *et al.*, *Phys. Rev. Lett.* **100**, 205701 (2008).
- [8] B. Thielemann *et al.*, *Phys. Rev. Lett.* **102**, 107204 (2009).
- [9] R. Coldea *et al.*, *Science* **327**, 177 (2010).
- [10] C.-L. Hung, X. Zhang, N. Gemelke, and C. Chin, *Nature* **470**, 236 (2011).
- [11] X. Zhang, C.-L. Hung, S.-K. Tung, and C. Chin, *Science* **335**, 1070 (2012).
- [12] M. Klanjšek *et al.*, *Phys. Rev. Lett.* **101**, 137207 (2008).
- [13] S. Sachdev, T. Senthil and R. Shankar, *Phys. Rev. B* **50**, 258 (1994).
- [14] T. Giamarchi, *Quantum Physics in One Dimension* (Oxford Univ. Press, Oxford, 2004).
- [15] Y. Maeda, C. Hotta, and M. Oshikawa, *Phys. Rev. Lett.* **99**, 057205 (2007).
- [16] C. Rüegg *et al.*, *Phys. Rev. Lett.* **101**, 247202 (2008).
- [17] A. Paduan-Filho, R. D. Chirico, K. O. Joung, and R. L. Carlin, *J. Chem. Phys.* **74**, 4103 (1981).
- [18] V. S. Zapf *et al.*, *Phys. Rev. Lett.* **96**, 077204 (2006).
- [19] S. A. Zvyagin *et al.*, *Phys. Rev. Lett.* **98**, 047205 (2007).
- [20] B. C. Watson *et al.*, *Phys. Rev. Lett.* **86**, 5168 (2001).
- [21] B. Thielemann *et al.*, *Phys. Rev. B* **79**, 020408 (2009).
- [22] E. Orignac, R. Citra, and T. Giamarchi, *Phys. Rev. B* **75**, 140403(R) (2007).
- [23] T. Moriya, *Prog. Theor. Phys.* **16**, 23 (1956).
- [24] S. Mukhopadhyay *et al.* (unpublished).
- [25] T. Giamarchi and A. M. Tsvelik, *Phys. Rev. B* **59**, 11398 (1999).
- [26] T. Nikuni, M. Oshikawa, A. Oosawa, and H. Tanaka, *Phys. Rev. Lett.* **84**, 5868 (2000).
- [27] T. Giamarchi, C. Rüegg, and O. Tchernyshyov, *Nature Phys.* **4**, 198 (2008).
- [28] D. Stauffer, M. Ferer, and M. Wortis, *Phys. Rev. Lett.* **29**, 345 (1972).
- [29] H. Kühne *et al.*, *Phys. Rev. B* **83**, 100407(R) (2011).